

Multimodal correlation of dynamic [^{18}F]-AV-1451 perfusion PET and neuronal hypometabolism in [^{18}F]-FDG PET

Jochen Hammes¹  · Isabel Leuwer¹ · Gérard N. Bischof^{1,2} · Alexander Drzezga^{1,3} · Thilo van Eimeren^{1,2,3}

Received: 1 August 2017 / Accepted: 22 September 2017 / Published online: 12 October 2017
© Springer-Verlag GmbH Germany 2017

Abstract

Purpose Cerebral glucose metabolism measured with [^{18}F]-FDG PET is a well established marker of neuronal dysfunction in neurodegeneration. The tau-protein tracer [^{18}F]-AV-1451 PET is currently under evaluation and shows promising results. Here, we assess the feasibility of early perfusion imaging with AV-1451 as a substitute for FDG PET in assessing neuronal injury.

Methods Twenty patients with suspected neurodegeneration underwent FDG and early phase AV-1451 PET imaging. Ten one-minute timeframes were acquired after application of 200 MBq AV-1451. FDG images were acquired on a different date according to clinical protocol. Early AV-1451 timeframes were coregistered to individual FDG-scans and spatially normalized. Voxel-wise intermodal correlations were calculated on within-subject level for every possible time window. The window with highest pooled correlation was considered optimal. Z-transformed deviation maps (ZMs) were created from both FDG and early AV-1451 images, comparing against FDG images of healthy controls.

Results Regional patterns and extent of perfusion deficits were highly comparable to metabolic deficits. Best results were observed in a time window from 60 to 360 s ($r = 0.86$). Correlation strength ranged from $r = 0.96$ (subcortical gray matter) to 0.83 (frontal lobe) in regional analysis. ZMs of early AV-1451 and FDG images were highly similar.

Conclusion Perfusion imaging with AV-1451 is a valid biomarker for assessment of neuronal dysfunction in neurodegenerative diseases. Radiation exposure and complexity of the diagnostic workup could be reduced significantly by routine acquisition of early AV-1451 images, sparing additional FDG PET.

Keywords Av-1451 · Tau-imaging · Cerebral perfusion · Cerebral FDG metabolism · Neurodegeneration

Introduction

Molecular imaging of pathologically misfolded and hyperphosphorylated tau-protein aggregations is of increasing interest with regard to the understanding of Alzheimer's disease (AD) [1–3], frontotemporal lobar degeneration (FTLD) [4, 5], progressive supranuclear palsy (PSP) and other neurodegenerative diseases [6–9]. The tau-protein binding properties of THK-5351 [10], AV-1451 (formerly known as T807) [11], PBB-3, MK-6240 [12] and others, are currently under investigation and show promising results, especially in AD. However, all tracers can still be considered in an exploratory stage [13] and the specificity of the binding of some tracers is under ongoing discussion. Ng et al. have shown in vivo that the binding of THK-5351 is reduced by the selective MAO-B inhibitor selegiline [14], and therefore it is now assumed that binding to MAO-B may be a source of off-target binding in THK-5351 [15]. Whether this is the case for other tau tracers remains unclear.

In addition to the detection of underlying pathology with specific molecular imaging or the analysis of cerebrospinal fluid, FDG PET is a well-established method for assessing the extent and spatial distribution of neuronal injury and has been in use for more than three decades [16, 17]. Because of

✉ Jochen Hammes
jochen.hammes@uk-koeln.de

¹ Multimodal Neuroimaging Group, Department of Nuclear Medicine, University Hospital Cologne, Cologne, Germany

² INM-3, Research Center Jülich, Jülich, Germany

³ German Center for Neurodegeneration (DZNE), Berlin, Germany

neurovascular coupling, there is a close correspondence of regional brain metabolism and regional perfusion [18]; comparative studies between glucose metabolism and perfusion imaging in neurodegenerative that show a similarity of defect patterns date back to the early 1990s [19].

A high correspondence between perfusion imaging, i.e. early acquisition windows of most of the available amyloid tracers, and FDG metabolism has also been shown in several studies [20–24], and early phase FP-CIT-acquisition windows show promising results in the differential diagnosis of Parkinsonian syndromes [25]. In addition, a substantial overlap between MR-based perfusion imaging with arterial spin labeling and metabolic imaging with FDG has been demonstrated [26]. Rodriguez-Vieitez et al. have recently shown that perfusion images of the tau-tracer THK-5317 are highly correlated with the FDG images of the respective patients [27].

This study investigates whether it is feasible to use perfusion imaging with the tau tracer AV-1451 as a proxy variable for neuronal glucose metabolism and as a measure of neuronal injury in patients with neurodegenerative diseases. If this were the case, imaging studies investigating the load of tau protein aggregations in AD and other neurodegenerative diseases with this tracer could easily include information on the extent of neuronal damage without having to apply a second imaging modality, sparing the patient from a second visit and from additional exposure to radiation. In this study we did not focus on a single disease entity, but investigated the applicability of AV-1451 perfusion imaging in a broad spectrum of suspected diagnoses.

Methods

Patients

Twenty subjects underwent PET imaging in the clinical workup of a suspected neurodegenerative disease (8 suspected AD, 7 suspected FTLT, 3 suspected PSP, 2 suspected corticobasal degeneration (CBD)). The study was carried out in accordance with the International Ethical Guidelines and Declaration of Helsinki.

Imaging

PET scans were performed at the Department of Nuclear Medicine, University Hospital Cologne, Germany, with a Siemens Biograph mCT Flow 128 Edge scanner (Siemens, Knoxville, TN) from November 2016 to March 2017. All 20 patients underwent biphasic AV-1451 imaging. Patients were placed in the scanner and a low-dose CT scan for the purpose of attenuation correction was acquired. PET image acquisition began directly after the injection of [¹⁸F]-AV-1451 (average activity 227 MBq, standard deviation 32 MBq). Ten image frames of 60 s each were acquired. The patients were asked to lie still

and to keep their eyes closed during the PET acquisition. The light in the scanner room was dimmed and any loud noise was avoided. After a pause of 80 min, an additional static image was acquired over 15 min. Images of the late acquisition window were not analyzed in this study. Of the patients, 18 underwent FDG PET imaging on another day in our department (average time between scans 24 days, standard deviation 33 days) according to clinical protocol with [¹⁸F]-FDG (average activity 212 MBq, standard deviation 18 MBq). After the injection of the tracer, patients waited for 30 min lying in supine position in a room with dimmed light. After that, patients were transferred to the scanner and a static image was acquired over 15 min. In two cases, the FDG PET scan was performed in external departments on different scanner types (GE Discovery STE and Siemens Biograph 6 True Point) within a two-month time window prior to the AV-1451 scan.

All PET scans from our department were iteratively reconstructed using a 3-D OSEM algorithm (four iterations, 12 subsets, Gaussian filter: 5 mm full width at half maximum (FWHM), 400 × 400 matrix, slice thickness of 3 mm, attenuation correction based on a low-dose CT).

All external scans were acquired in a clinical setting and reconstructed using an iterative reconstruction algorithm and CT-based attenuation correction. Where not already present, external images were smoothed according to the protocol from our department.

Early [¹⁸F]-AV-1451 images were coregistered to the FDG PET scan of the respective patient. The FDG scans were then spatially normalized to MNI space [28] to the standard PET template included with SPM 12 (www.fil.ion.ucl.ac.uk/spm/software/spm12). The transformation parameters acquired in this process were also applied to the early [¹⁸F]-AV-1451 frames that were in register with the FDG images. The resulting image resolution was 2x2x2 mm³ with matrix dimensions of 79x95x78 voxels.

A cubic linear smoothing kernel with a radius of 3 voxels was applied to the images. Since perfusion or glucose metabolism should be assessed only in gray matter (GM), the images were multiplied with a binary GM mask. This mask was created based on the SPM probabilistic GM map. A threshold of a GM probability of 0.5 was chosen after visual anatomical inspection of the probabilistic map. For every patient, voxel-wise intra-subject correlation coefficients were calculated for every possible time frame in the window from 0 to 600 s using a custom-built Matlab script (The MathWorks, Inc., Natick, MA). To pool the correlation coefficients over the entire set of patients, Fisher's Z-transformations were calculated according to the formula

$$z_f(r) = \frac{1}{2} \ln \left(\frac{1+r}{1-r} \right) \quad (1)$$

z_f : Fisher's Z-Transform, r : correlation coefficient [29].

Pooled Z-transformed correlation coefficients were back-transformed according to

$$r(z_f) = \frac{\exp(2z_f - 1)}{\exp(2z_f + 1)} = \tanh z_f \quad (2)$$

Pooled correlations coefficients were calculated for the whole brain and lobe-wise according to the Hammers probabilistic atlas for cortical areas (<http://www.brain-development.org>) [30] and according to the Harvard-Oxford Atlas for subcortical areas [31]. The optimal acquisition time was determined by identification of the time window with the highest back-transformed pooled correlation coefficient.

To determine the spatial distribution of the correlation strength, a between-subject correlation coefficient based on the 20 data pairs of FDG and early AV-1451 PET signals was calculated for every voxel. Sum-images of the optimal time window were intensity standardized by SUVR calculation with the cerebellum defined in the AAL atlas [32] as a reference region and smoothed with a cubic linear smoothing kernel with a radius of 3 mm. Since statistical correlation strength is dependent on the variance in the underlying data, voxel-wise between-subject standard deviation in the FDG signal was calculated, as well.

For each of the tracers (FDG images and the early AV-1451 sum-images, respectively), two series of SUVR image-datasets were created, one using the cerebellum and another one using the whole brain as reference regions. These normalized images were then individually compared against a mean image of a set of FDG scans from 18 older healthy controls. Individual deviations from the norm cohort were then Z-transformed as described previously [1]. To depict the average concordance between early AV-1451 and FDG deviation maps and to assess the feasibility of creating Z-transformed deviation maps from early [^{18}F]-AV-1451 images with a set of FDG control data, voxel-wise paired T-tests were performed to identify areas of significant differences between Z-transformed deviation maps of the FDG scans and the early [^{18}F]-AV-1451 scans for the images created both with cerebellar and whole brain as reference regions. FWE-corrected p -values <0.05 were considered significant.

Early [^{18}F]-AV-1451 sum-images of the optimal time window and the FDG PET scans of the respective patients were also processed with NEUROSTAT [33] and compared visually. Image display and 3D volume renderings were produced in VINCI 4 [34] and Mango (<http://ric.uthscsa.edu/mango/index.html>).

To investigate the dependency of suspected diagnosis on correlation strength, a two sample t-test was performed comparing the Fisher's Z-transformed correlation coefficients from the optimal time window of the AD and the FTL D group. CBD and PSP patients were not included in this analysis due to the low number of patients ($n_{\text{CBD}} = 2$, $n_{\text{PSP}} = 3$).

Results

Voxel-wise pooled whole-cortex intrasubject correlation coefficients for every possible time window are depicted in Table 1. Table 2 shows the highest correlation coefficients and optimal time window for the VOI-wise analysis. Highest correlation coefficients were observed in summed images for the time window from 60 to 360 s in parietal, temporal and occipital lobe and in the whole-cortex analysis. In subcortical GM, voxel-wise intra-subject coefficients were even higher than in cortical GM. Only in the brain stem VOI was the correlation between FDG and perfusion signal comparatively poor. The average correlation strength did not differ between the AD and the FTL D group ($p = 0.19$).

Figure 1 depicts the voxel-wise intra-subject dependency between FDG and AV-1451 perfusion signal for one exemplary patient with suspected Alzheimer's disease in several time windows. A clear linear dependency is present in all time windows later than 60 s after the injection of the tracer. The additional signal component in Fig. 1B (red) depicts the interference caused by extra-cerebral voxels, probably stemming from cranial soft tissue with a lower glucose metabolism rate in comparison to the cerebral cortex.

Figure 2 shows the high visual similarity of the FDG-scan of one patient with suspected Alzheimer's disease in comparison to the AV-1451 sum-image in the optimal time window.

The visual similarity of 3D stereotactic surface projections of Z-transformed deviations from an FDG-norm cohort of individual early AV-1451 and FDG images in one patient with suspected Alzheimer's disease is shown in Fig. 3A for both cerebellum and whole brain as reference regions in SUVR-creation. Figure 3B depicts the average concordance between early AV-1451 and FDG Z-deviation maps. When using the whole brain as the reference region in SUVR-creation, only areas in the central region and the primary visual cortex show significantly higher Z-scores in the early AV-1451-based data as compared to the FDG-based data in a voxel-wise paired T-test. When using the cerebellum as a reference region, significant differences are more widely spread. Here, early AV-1451 Z-scores are higher in the central region, in major portions of the occipital cortex, in the superior temporal cortex and in frontolateral areas. Cortical FDG Z-scores were not higher than early AV-1451 Z-scores in any case.

The regional distribution of voxel-wise between-subject correlations of PET SUVRs is shown in Fig. 4A. High correlation coefficients are present throughout the cortex, except for the ventral parts of the central region, pons and brainstem. Figure 4B depicts the dependency of voxel-wise between-subject correlation and standard deviation in FDG signal across the 20 patients as a measure of variance in the underlying data and the probability of the respective voxel belonging to GM (only voxels with a GM probability were included in the correlation analysis). Voxels with a high GM probability

Table 1 Voxel-wise pooled intra-subject correlation coefficients for every possible time window, whole cortex VOI

End→	60 s	120 s	180 s	240 s	300 s	360 s	420 s	480 s	540 s	600 s
Start↓										
0 s	0.519	0.778	0.833	0.852	0.861	0.863	0.863	0.861	0.859	0.855
60 s		0.801	0.846	0.860	0.865	0.866	0.865	0.863	0.859	0.856
120 s			0.816	0.849	0.858	0.860	0.859	0.857	0.854	0.850
180 s				0.814	0.842	0.849	0.850	0.849	0.846	0.842
240 s					0.804	0.831	0.838	0.839	0.837	0.833
300 s						0.792	0.819	0.826	0.826	0.824
360 s							0.781	0.808	0.813	0.813
420 s								0.768	0.794	0.798
480 s									0.752	0.777
540 s									0.000	0.733

generally show high correlation coefficients. In voxels with enough variance in the FDG data, only high correlation coefficients were found. Only in low-GM-probability areas and areas with low variance of FDG metabolism in the underlying sample were the correlation coefficients poor.

Discussion

In this study, we show for the first time the feasibility of [¹⁸F]-AV-1451 imaging in early acquisition windows as a marker of cerebral perfusion. A region-specific correlation analysis yielded high correlation coefficients for cortical and subcortical areas and identified the time from 60 to 360 s as an optimal time window where correlation was strongest. However, correlation coefficients in other time frames between 60 and 600 s were only slightly lower. AV-1451 sum-images from the optimal time window proved to have very high visual similarity to FDG images acquired according to a standard clinical protocol. The same image processing pipeline used in creating 3D

stereotactic surface projections for the assessment of the regional pattern of the neuronal injury could be used for both set of images.

The high correlation and the clear-cut visual similarity between perfusion imaging and metabolic imaging with FDG has been shown in many prior studies [19, 26, 27], and is caused by the mechanisms of neurovascular coupling [18]. In our study, the striking overlap between perfusion imaging with early AV-1451 and metabolic imaging with FDG was demonstrated to even allow the calculation of voxel-wise deviation maps in comparison to the same FDG-based norm cohort. However, our data show, strength and distribution of regional perfusion and glucose metabolism are not identical. The similarity of deviation patterns is highest when the whole brain is used as the reference region, whereas differences in Z-scores are higher in deviation maps calculated with the cerebellum as the reference region. This finding is probably caused by a difference of relative cortico-subcortical perfusion and cortico-subcortical metabolism. Differences between relative regional metabolism and perfusion have been reported in previous studies in the cerebellum, pons and some cortical regions [35]. Our data suggest that the relative perfusion of subcortical GM in comparison to cortical areas is higher than the relative FDG metabolism. These differences result in artificially increased cortical Z-transformed deviations when perfusion images are compared to a set of normal controls and a subcortical reference region is selected for the creation of SUVR images.

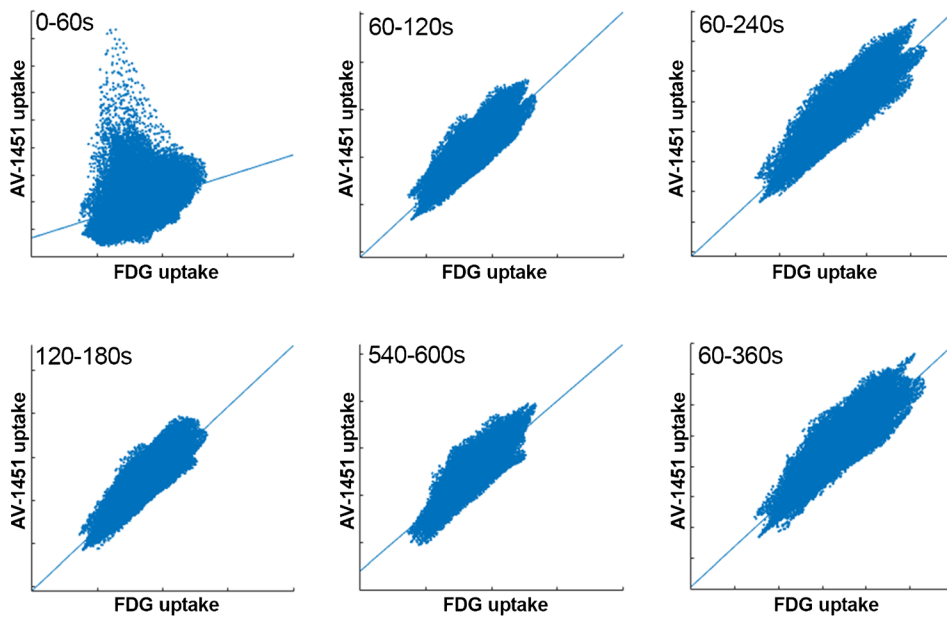
Dissimilarities between early AV-1451 perfusion images and FDG images might also be influenced by differences of experimental conditions in the environment of the patients. While FDG scans were acquired after the patient waited for 30 min lying in supine position in a quiet room with dimmed light, naturally, the perfusion phase was acquired while the patient was situated in the scanner and therefore being exposed to a higher level of auditory and visual input. However, we did not find a significant increase of relative

Table 2 highest intra-subject pooled correlation coefficients in lobe-wise analysis

VOI	Optimal acquisition window	Highest pooled intra-subject correlation coefficient	Pooled intra-subject correlation coefficient in 60–360 s window
frontal	60–300 s	0.826	0.822
temporal	60–360 s	0.854*	0.854*
parietal	60–360 s	0.879*	0.879*
occipital	60–360 s	0.898*	0.898*
basal ganglia	60–540 s	0.959	0.955
thalamus	60–480 s	0.958	0.956
brain stem	60–480 s	0.669	0.653
whole-cortex	60–360 s	0.866*	0.866*

* highest correlation occurred in optimal-acquisition window

a with GM mask



b without GM mask

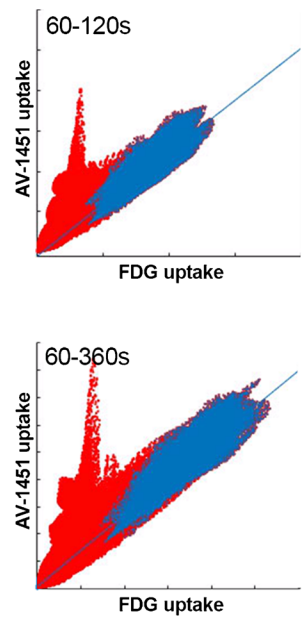


Fig. 1 Voxel-wise Intra-subject correlations for different time windows in an exemplary patient with suspected Alzheimer’s disease. A: Only voxels with a GM probability >0.5 included; B: No mask applied, voxels with GM probability <0.5 are shown in red

activation in the visual and auditory cortices comparing perfusion and FDG images.

It is possible that the early AV-1451 images might be affected by the heterogeneous distribution tau depositions

across regions. This effect would result in artificially increased perfusion signals in areas of high tau protein densities and, in turn, in a decrease of correlation strength between FDG and early AV-1451. As eight of the patients analyzed in this study

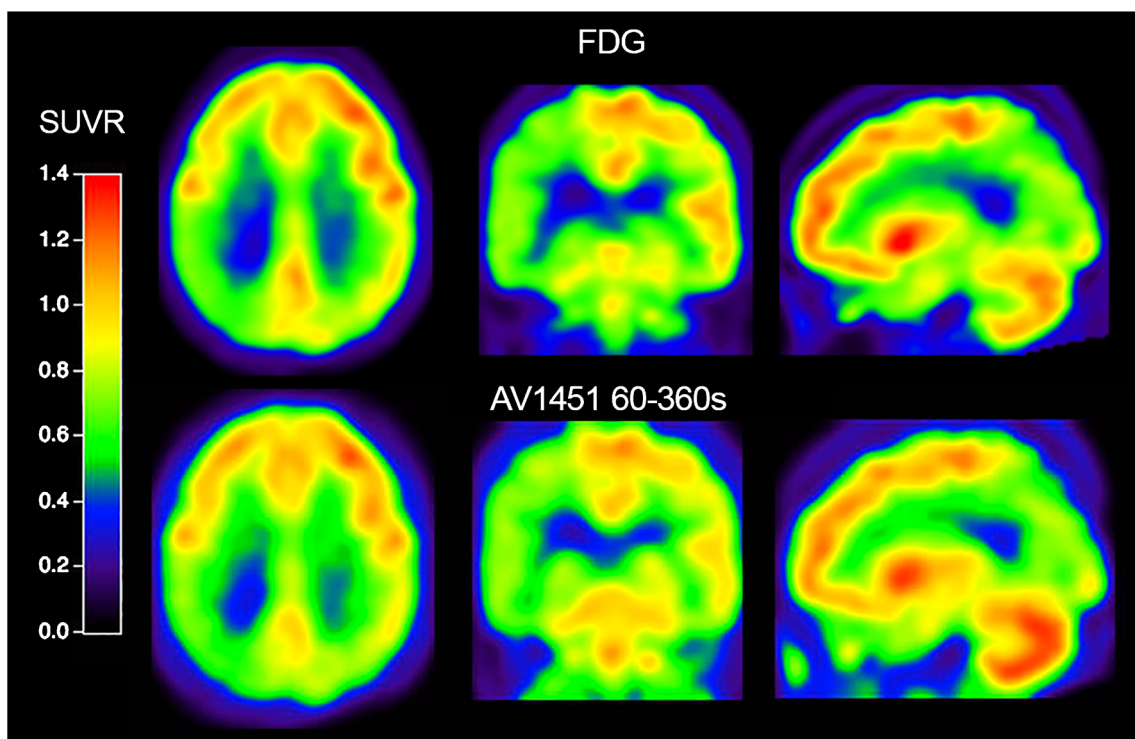


Fig. 2 Exemplary images of one patient with suspected Alzheimer’s disease showing high visual similarity of the pattern of hypometabolism in FDG PET and pattern of hypoperfusion in early AV-1451 image

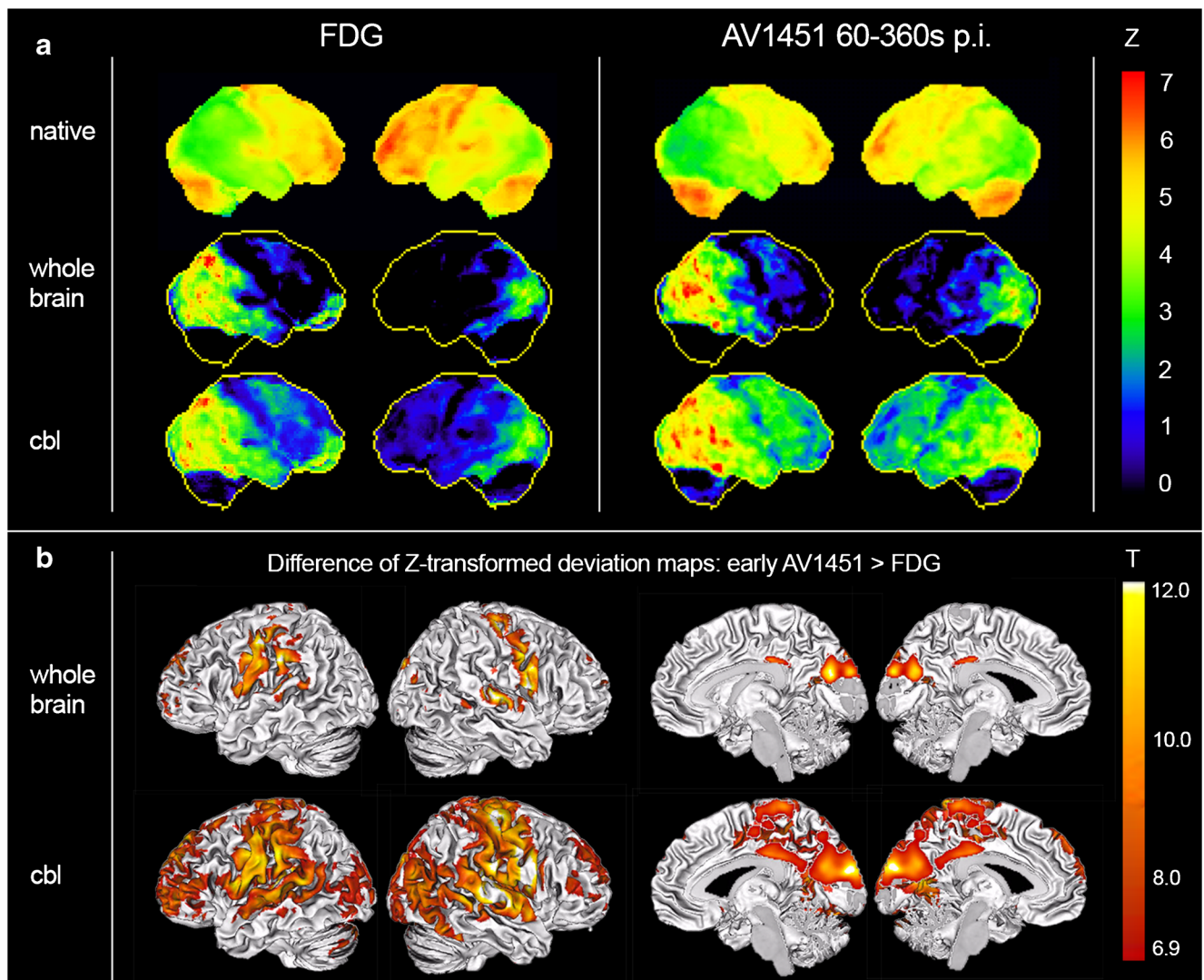


Fig. 3 A) 3D–stereotactic surface projections (NEUROSTAT) depicting regional distribution of Z-transformed deviations of FDG and early AV-1451 images from a norm cohort in one individual with suspected

Alzheimer’s disease. B) Group analysis with voxel-wise paired T-Test comparing Z-transformed deviations of early AV-1451 and FDG images from a norm cohort

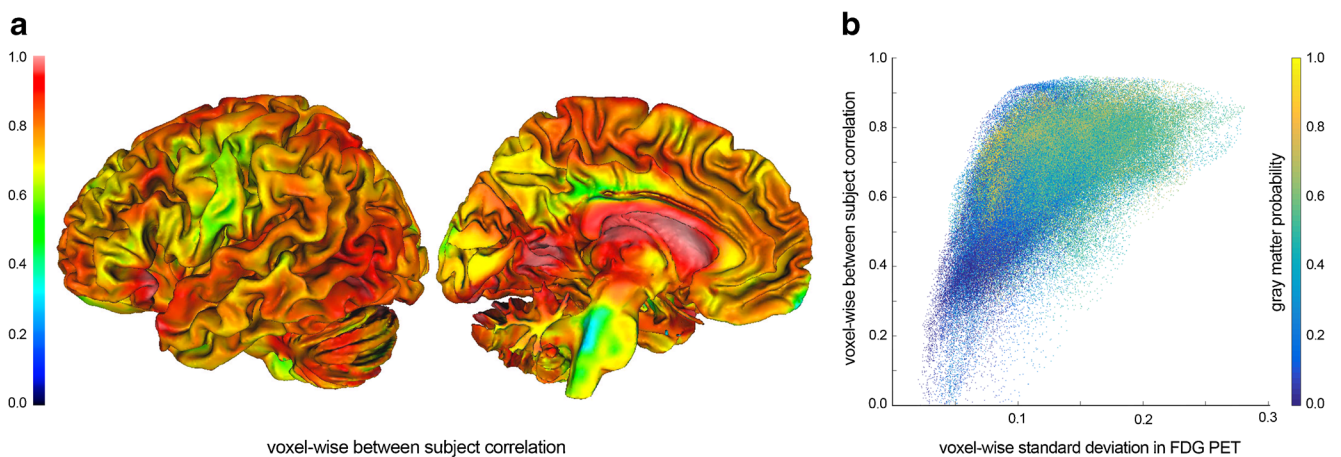


Fig. 4 A: Regional distribution of correlation strength depicted by voxel-wise between-subject correlation, B: dependency of voxel-wise between-subject correlation and standard deviation in FDG signal and probability of the respective voxel belonging to GM

were suspected AD patients and seven were suspected FTLN patients, one would expect a relative decrease in regional correlation strength in temporo-parietal and frontal areas if this effect was strong. However, Figs. 3B and 4 show a rather strong regional correlation strength in these areas, suggesting that the influence of specific binding of AV-1451 to tau protein aggregation has a negligible influence on the perfusion signal.

Hsiao and Lin et al. have previously described that the highest correlation strength between Florbetapir perfusion imaging and FDG imaging is also present in a window from 60 to 360 s [23, 24], while Jin et al. have found the window from 60 to 600 s to be optimal when acquiring perfusion images with FP-CIT [25]. According to Rodriguez-Vieitez the Tau-tracer THK-5317 is best suited as a perfusion marker in a very early time window of 0–180 s, while they have also observed high correlation coefficients in later time frames. They concluded that the time window for SUVR-creation images could be determined locally as a function of preference [27]. Taking our findings into account, we agree with Rodriguez-Vieitez, as the correlation strengths do not vary much when increasing or decreasing the acquisition time by 60–120 s. However, considering that the influence of specific binding of the tracer to tau protein aggregations could potentially increase with time after injection, we would recommend using early time windows.

In the analysis of the regional distribution of the correlation strength, comparatively poor results were obtained for the brainstem and the pons. This is of particular importance as the pons is commonly used as a reference region for SUVR-creation in FDG imaging. Based on the data of this study, the pons should not be used for SUVR-creation of perfusion imaging.

Since this study focuses on a technical comparison between imaging modalities, it does not include an analysis of the individual rater-based diagnostic accuracy of the two techniques. However, the striking concordance of AV-1451 perfusion and FDG metabolic images both natively and in Z-transformed deviation maps suggest that early AV151 imaging is feasible for assessing patterns of regional neuronal injury. The intra-subject correlation coefficients that were even higher in the basal ganglia are especially promising with respect to patients with suspected atypical Parkinsonian syndromes.

As for AD patients, there seems to be a strong negative correlation between FDG metabolism and tau pathology measured in AV-1451 PET [2, 36], so that the additional information on regional extent of pathology gained by imaging the neuronal dysfunction might be limited in these patients. However, data from our and other groups suggest that tau-abnormalities may precede neuronal dysfunction in prodromal and early stages of the disease, stressing the diagnostic relevance of a combination of both modalities [13, 37]. Moreover, the binding properties of AV-1451 in other neurodegenerative

diseases are different from those in AD [4, 5], and therefore drawing conclusions on neuronal dysfunction only from late acquisition windows of this tau tracer would not be valid in these cases.

Conclusion

Early acquisition windows of AV-1451 PET seem to be a valid biomarker for assessing the extent and regional distribution of neuronal dysfunction in neurodegenerative diseases. Highest voxel-wise correlations to the gold standard FDG PET are found in a time window from 60 to 360 s after intravenous injection of the tracer. By routinely acquiring perfusion images and consequently sparing the patient an additional FDG PET scan, radiation exposure and complexity of the diagnostic workup could be reduced significantly.

Compliance with ethical standards All procedures performed in studies involving human participants were in accordance with the ethical standards of the institutional and/or national research committee and with the 1964 Helsinki declaration and its later amendments or comparable ethical standards.

This article does not contain any studies with animals performed by any of the authors.

Informed consent Informed consent was obtained from all individual participants included in the study.

Conflict of interest IL, GNB and JH report no potential conflicts of interest. AD received consulting and speaker honoraria and research support from Siemens Healthcare, AVID Radiopharmaceuticals, Lilly, Piramal, and GE Healthcare. TvE received lecture fees from Lilly Germany, and research funding from the German Research Foundation (DFG), the Leibniz Association and the EU-joint program for neurodegenerative disease research (JPND).

References

1. Bischof GN, Jessen F, Fliessbach K, et al. Impact of tau and amyloid burden on glucose metabolism in Alzheimer's disease. *Ann Clin Transl Neurol.* 2016;3:934–9.
2. Dronse J, Fliessbach K, Bischof GN, et al. In vivo Patterns of Tau Pathology, Amyloid- β Burden, and Neuronal Dysfunction in Clinical Variants of Alzheimer's Disease. *J Alzheimers Dis.* 2016: 1–7.
3. Johnson KA, Schultz A, Betensky RA, et al. Tau positron emission tomographic imaging in aging and early Alzheimer disease. *Ann Neurol.* 2016;79:110–9.
4. Spina S, Schonhaut DR, Boeve BF, et al. Frontotemporal dementia with the V337M MAPT mutation: Tau-PET and pathology correlations. *Neurology.* 2017;88:758–66.
5. Dani M, Brooks DJ, Edison P. Tau imaging in neurodegenerative diseases. *Eur J Nucl Med Mol Imaging.* 2016;43:1139–50.
6. Hammes J, Bischof GN, Giehl K, et al. Elevated in vivo [18F]-AV-1451 uptake in a patient with progressive supranuclear palsy. *Mov Disord.* 2017;32:170–1.

7. Cho H, Choi JY, Hwang MS, et al. Subcortical (18) F-AV-1451 binding patterns in progressive supranuclear palsy. *Mov Disord.* 2017;32:134–40.
8. Whitwell JL, Lowe VJ, Tosakulwong N, et al. [18F]AV-1451 tau positron emission tomography in progressive supranuclear palsy. *Mov Disord.* 2017;32:124–33.
9. Smith R, Schain M, Nilsson C, et al. Increased basal ganglia binding of (18) F-AV-1451 in patients with progressive supranuclear palsy. *Mov Disord.* 2017;32:108–14.
10. Betthausen T, Lao PJ, Murali D, et al. In vivo comparison of tau radioligands 18F-THK-5351 and 18F-THK-5317. *J Nucl Med.* 2017;58:996–1002.
11. Xia C-F, Arteaga J, Chen G, et al. [18F]T807, a novel tau positron emission tomography imaging agent for Alzheimer's disease. *Alzheimers Dement.* 2013;9:666–76.
12. Walji AM, Hostetler ED, Selnick H, et al. Discovery of 6-(Fluoro-(18)F)-3-(1H-pyrrolo[2,3-c]pyridin-1-yl)isoquinolin-5-amine ([18F]-MK-6240): A positron emission tomography (PET) imaging agent for quantification of neurofibrillary tangles (NFTs). *J Med Chem.* 2016;59:4778–89.
13. van Eimeren T, Bischof GN, Drzezga AE. Is tau imaging more than just 'upside-down' FDG imaging? *J Nucl Med*; Epub ahead of print 10 May 2017. <https://doi.org/10.2967/jnumed.117.190082>.
14. Ng KP, Pascoal TA, Mathotaarachchi S, et al. Monoamine oxidase B inhibitor, selegiline, reduces 18F-THK5351 uptake in the human brain. *Alzheimers Res Ther*; 9. Epub ahead of print 31 March 2017. <https://doi.org/10.1186/s13195-017-0253-y>.
15. Saint-Aubert L, Lemoine L, Chiotis K, et al. Tau PET imaging: present and future directions. *Mol Neurodegener.* 2017;12:19.
16. Teipel S, Drzezga A, Grothe MJ, et al. Multimodal imaging in Alzheimer's disease: validity and usefulness for early detection. *Lancet Neurol.* 2015;14:1037–53.
17. Heiss WD, Herholz K, Pawlik G, et al. Positron emission tomography as a quantitative imaging method for demonstrating regional brain metabolism. *Digitale Bilddiag.* 1984;4:37–45.
18. Phillips AA, Chan FH, Zheng MMZ, et al. Neurovascular coupling in humans: Physiology, methodological advances and clinical implications. *J Cereb Blood Flow Metab.* 2016;36:647–64.
19. Mielke R, Pietrzyk U, Jacobs A, et al. HMPAO SPET and FDG PET in Alzheimer's disease and vascular dementia: comparison of perfusion and metabolic pattern. *Eur J Nucl Med.* 1994;21:1052–60.
20. Tiepolt S, Hesse S, Patt M, et al. Early [18F]florbetaben and [11C]PiB PET images are a surrogate biomarker of neuronal injury in Alzheimer's disease. *Eur J Nucl Med Mol Imaging.* 2016;43:1700–9.
21. Rostomian AH, Madison C, Rabinovici GD, et al. Early 11C-PIB frames and 18F-FDG PET measures are comparable: A study validated in a cohort of AD and FTLT patients. *J Nucl Med.* 2011;52:173–9.
22. Meyer PT, Hellwig S, Amtage F, et al. Dual-biomarker imaging of regional cerebral amyloid load and neuronal activity in dementia with PET and 11C-labeled Pittsburgh compound B. *J Nucl Med.* 2011;52:393–400.
23. Lin K-J, Hsiao I-T, Hsu J-L, et al. Imaging characteristic of dual-phase 18F-florbetapir (AV-45/Amyvid) PET for the concomitant detection of perfusion deficits and beta-amyloid deposition in Alzheimer's disease and mild cognitive impairment. *Eur J Nucl Med Mol Imaging.* 2016;43:1304–14.
24. Hsiao I-T, Huang C-C, Hsieh C-J, et al. Correlation of early-phase 18F-florbetapir (AV-45/Amyvid) PET images to FDG images: preliminary studies. *Eur J Nucl Med Mol Imaging.* 2012;39:613–20.
25. Jin S, Oh M, Oh SJ, et al. Additional value of early-phase 18F-FP-CIT PET image for differential diagnosis of atypical parkinsonism. *Clin Nucl Med.* 2017;42:e80–7.
26. Verfaillie SCJ, Adriaanse SM, Binnewijzend MAA, et al. Cerebral perfusion and glucose metabolism in Alzheimer's disease and frontotemporal dementia: two sides of the same coin? *Eur Radiol.* 2015;25:3050–9.
27. Rodriguez-Vieitez E, Leuzy A, Chiotis K, et al. Comparability of [18F]THK5317 and [11C]PiB blood flow proxy images with [18F]FDG positron emission tomography in Alzheimer's disease. *J Cereb Blood Flow Metab.* 2016; **0271678X16645593**
28. Evans AC, Collins DL, Mills SR, et al. 3D statistical neuroanatomical models from 305 MRI volumes. In: *Nuclear Science Symposium and Medical Imaging Conference, 1993., 1993 I.E. Conference Record.* 1993, pp. 1813–1817 vol.3.
29. Fisher RA. Frequency distribution of the values of the correlation coefficient in samples from an indefinitely large population. *Biometrika.* 1915;10:507–21.
30. Hammers A, Allom R, Koeppe MJ, et al. Three-dimensional maximum probability atlas of the human brain, with particular reference to the temporal lobe. *Hum Brain Mapp.* 2003;19:224–47.
31. Makris N, Goldstein JM, Kennedy D, et al. Decreased volume of left and total anterior insular lobule in schizophrenia. *Schizophr Res.* 2006;83:155–71.
32. Tzourio-Mazoyer N, Landeau B, Papathanassiou D, et al. Automated anatomical labeling of activations in SPM using a macroscopic anatomical parcellation of the MNI MRI single-subject brain. *NeuroImage.* 2002;15:273–89.
33. Minoshima S, Frey KA, Koeppe RA, et al. A diagnostic approach in Alzheimer's disease using three-dimensional stereotactic surface projections of Fluorine-18-FDG PET. *J Nucl Med.* 1995;36:1238–48.
34. Vollmar S, Čížek J, Sué M, et al. VINCI-volume imaging in neurological research, co-registration and ROIs included. In: Kremer K, Macho V, editors. *Forschung und wissenschaftliches Rechnen 2003.* Göttingen: GWDG; 2004. p. 115–31.
35. Wong CO, Thie J, Gaskill M, et al. A statistical investigation of normal regional intra-subject heterogeneity of brain metabolism and perfusion by F-18 FDG and O-15 H2O PET imaging. *BMC Nucl Med.* 2006;6:4.
36. Ossenkoppele R, Schonhaut DR, Schöll M, et al. Tau PET patterns mirror clinical and neuroanatomical variability in Alzheimer's disease. *Brain.* 2016;139:1551–67.
37. Schonhaut DR, Ossenkoppele R, Bejanin A, et al. Tau-pet patterns overlap and exceed hypometabolism in Alzheimer's disease. *Alzheimers Dement.* 2016;12:545–P547.